Tribology Letters (2023) 71:59
https://doi.org/10.1007/s11249-023-01731-6

ORIGINAL PAPER

n-Pentanol Lubrication of Silica Layers Passivated with Hydroxyl Groups Under Constant Shear Stress and Load and Isothermal Conditions

Roberto Guerra-Gonzalez[1] · Vidal Moises Bastida-Silva[2] · Jose Luis Rivera[3] · Fernando Iguazu Ramirez-Zavaleta[2] · Enrique Lima[3]

Received: 14 November 2022 / Accepted: 2 April 2023 / Published online: 19 April 2023

Abstract

We conducted molecular dynamics simulations to study the frictional behavior of hydroxyl-passivated silica layers lubricated with *n*-pentanol chains under constant shear stress, constant normal load, and isothermal conditions. We analyzed the resulting single, multiple, and continuous sliding regimes for several shear stresses at a single normal load and proposed a sliding mechanism between the *n*-pentanol chains' methyl groups. The critical ordering of hydrogen bonds between hydroxyl groups on the surface and the lubricant is necessary to reach the stationary state, where velocity follows a logarithmic dependence on shear stress up to a critical speed of 20 nm/ns. Stationary states corresponding to pure single slip and continuous sliding behaviors showed normal speed distributions, while multiple slip behavior showed near normal and bimodal distributions. In the single slip behavior, layers show constant displacements of 0.27 Å, representing half the separation of two surface hydroxyls in the sliding direction. The lubricant experienced minor volume expansions throughout the range of studied shear stresses due to an increasing layer separation at the contact surface and increasing tilting of the lubricant chains.

Graphical Abstract

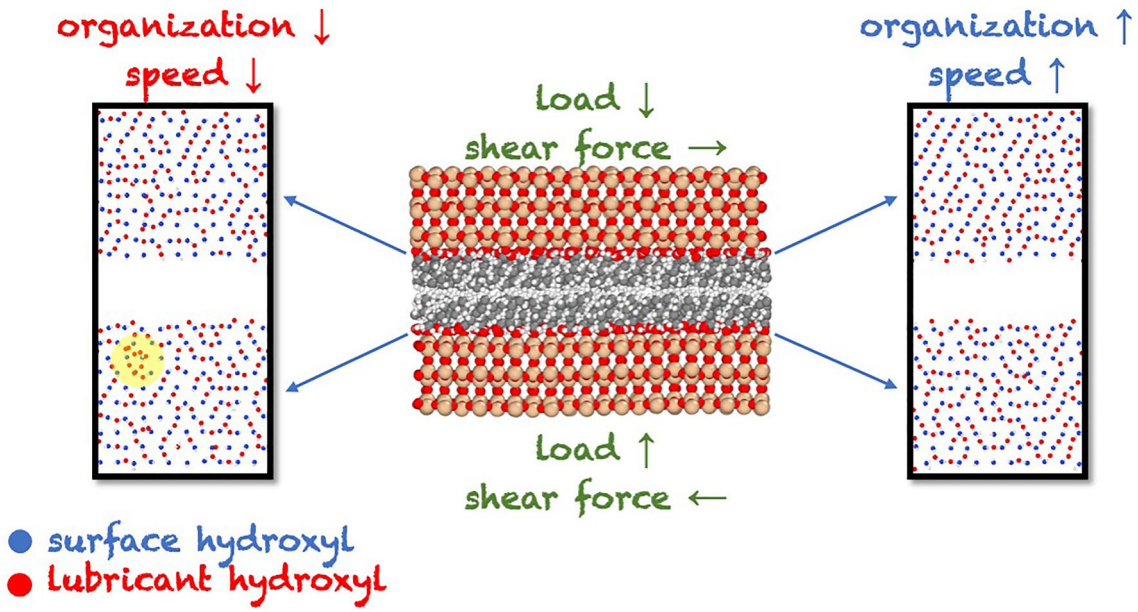

Keywords Vapor lubrication · Silica · Pentanol · Molecular dynamics · Organization · Stick - slip

Extended author information available on the last page of the article

1 Introduction

The in-situ vapor-phase lubrication of silica surfaces uses short-chain linear alcohols, such as *n*-alcohols, to produce reliable mechanical displacements for nano-electro-mechanical system (NEM) applications. The selection of *n*-alcohols is based on their ability to interact with passivated silica surfaces through hydrogen bonding [1–3]. This method is termed "in situ" because the surface modification responsible for low friction and wear prevention occurs automatically at the sliding contact created by the adsorbed monolayers, where sufficient lubricant molecules are present from the gas phase. Vapor phase lubrication has proven to be an effective means of protecting silica surfaces in NEMs that commonly have large adhesion contacts resulting from van der Waals dispersion forces, electrostatic interactions, and capillary phenomena [1]. In recent tests, an unprecedented NEM lifetime of 11 days was achieved in an environment close to *n*-pentanol vapor saturation, with the system stopped after 10^8 cycles [2]. This result was attributed to the ability of adsorbed *n*-pentanols to overcome silica's naturally high friction.

Molecular dynamics (MD) simulations are often used to investigate the sliding behavior of lubricated layers under normal load [4–6]. Simulations often impose a fixed separation constraint between the outermost layers to maintain a stationary state with a constant load, resulting in load fluctuations around a constant value [7–9]. The constant-separation approach is particularly advantageous when studying the sliding of a tip on surfaces since the alternative method of imposing constant external forces to mimic a constant load can lead to the bending of the layer with the larger area in the normal direction [10–12]. Additionally, simulations of rough or curved surfaces commonly use the constant-separation method to simplify the study of frictional phenomena [9]. Simulations of planar surfaces with the same area as those studied in this work can be performed using both methods. However, the constant-force approach can produce a wider range of mechanical states that are unachievable with the constant-separation method because, under constant force, layers are free to expand or contract when the load fluctuates around a constant value.

Simulations using constant separation or force to mimic a constant load are not equivalent, even when imposing the average value of the load obtained from constant-separation simulations in corresponding constant-force simulations and vice versa [13]. Constant-separation simulations result in a distribution of normal forces, which may require a comparable effective constant force rather than the average force from the constant-separation simulation, especially when the distribution of normal forces has a large variance. Both methods will likely provide comparable results for systems with macroscopic thicknesses because the contact surfaces are located far from the system boundaries (where the constraints are applied), and artifacts generated at the system's limits are less likely to be transmitted to the frictional surfaces.

Shear stress can be controlled in MD simulations using either constant sliding speed [14–16] or constant shear force [17–19]. In the constant sliding speed method, constant and opposite speeds are applied to the outermost plane of atoms in each layer, and chains have a constant time for physical bond formation and breaking, resulting in a frictional process. In the constant shear force method, external constant and opposite shear forces are applied to the outermost plane of atoms in each layer; physical bonds are formed and broken only when the energetic conditions are appropriate. However, like the control on the normal load, these methods may not be equivalent. An effective value must be used instead of the average value of the estimated variable to make them comparable. High variance in speed or shear stress can cause the sliding process to shift from a single slip to multiple slips or a continuous sliding behavior [20–22]. Additionally, MD under constant-speed conditions may develop artificial periodic stick and slip events [23], preventing multiple-slip events.

This study investigates the frictional behavior of silica layers passivated with hydroxyl groups that anchor *n*-pentanol lubricant chains, promoting sliding contact to the top of the adsorbed monolayers. The methodology section details load and shear stress control procedures, applied potentials, and simulation methods. The results section presents the temporal profiles of sliding regimes at varying shear stresses, analyzes key atoms' properties and spatial distributions, and examines the resulting stationary and temporal regimes.

2 Methodology

In this study, we investigated the frictional behavior of β-cristobalite silica, which has uniform planes suitable for use in nanomechanical devices' moving parts. These planes can terminate in an oxygen atom layer that can be passivated with hydrogen atoms, forming hydroxyl groups [24]. The planes have large coefficients of friction despite being passivated with hydrogen instead of hydroxyl groups. When two silica layers passivated with hydroxyl groups, interact and form hydrogen bonds that can withstand strong shear forces, preventing them from sliding. Alternatively, low coefficients of friction can be achieved using a lubricant chain (such as *n*-pentanols) with hydroxyl groups that interact with the surface hydroxyl groups through hydrogen bonds, eventually causing the

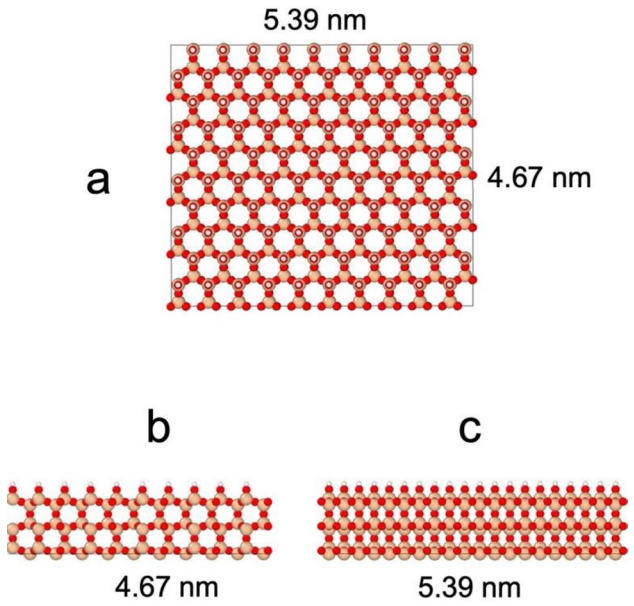

Fig. 1 **a** Normal view of plane (111) and **b–c** the side views of a sliding layer of silica (β-cristobalite) passivated with hydroxyl groups. Red, brown, and white spheres represent oxygen, silicon, and hydrogen atoms, respectively (Color figure online)

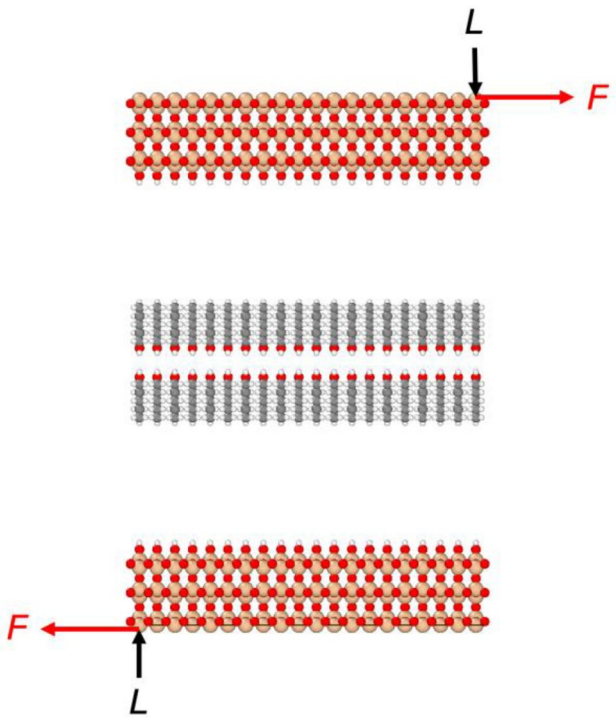

Fig. 2 Side view of the silica (β-cristobalite) layers passivated with hydroxyl groups and *n*-pentanol molecules as a lubricant (center). Each outermost silicon atom is exposed to a normal load (L) and a shear force (F). Red, brown, gray, and white spheres represent oxygen, silicon, carbon, and hydrogen atoms, respectively

contact surface to shift to the *n*-pentanol molecules' terminal methyl groups, which form monolayer coatings on the silica layers. Research on coated surfaces terminating in methyl groups has shown low coefficients of friction [25–27].

Figure 1a shows the (111) contact surfaces of β-cristobalite, which have terminal hydroxyl groups with the lowest surface hydroxyl group density compared to other uniform planes of β-cristobalite silica. First principles studies estimate that the (111) plane contains approximately 4.29 surface hydroxyl groups per nm^2 [28]. This density aligns with experimental measurements, indicating a consistent hydroxyl group density of 4.9 ± 0.6 per nm^2 regardless of the silica's surface topology or bulk phase [29].

MD simulations cannot fully replicate actual tribological processes due to computational limitations. Typically, simulations are restricted to very thin layers, such as those studied in this work (Fig. 1b and c), containing a contact area of 10×10 hydroxyl groups on each silica surface and thicknesses of a few nanometers. The simulated area remained constant while the systems were allowed to move in the normal direction. The initial conformation corresponded to the equilibrium conformation constructed using the interaction potential parameters previously used to investigate the frictional forces between amorphous silicon oxide surfaces coated with self-assembled perfluoroalkyl chains [30]. The density of the hydroxyl groups in the equilibrium conformation was ~ 3.97 hydroxyl groups per nm^2, which is 7.4% lower than that reported in previous first-principles calculations [28]. The simulations excluded additional effects arising from the roughness of the surfaces to isolate the pure tribological effect. While manufacturing processes minimize surface imperfections, these effects still dominate in many real systems of technological interest.

In this model, two layers with the same conformation but symmetrically opposed in the normal direction were brought into contact (Fig. 2) with two layers of *n*-pentanol molecules located between them and the lubricant's methyl groups pointing towards the silica layers. Due to computational limitations, *n*-pentanol molecules were not initially adsorbed at the silica surfaces forming saturated monolayers in thermodynamical equilibrium with a vapor phase. We initiated the simulation starting from the case (out of equilibrium) where silica layers are separated, not in mechanical contact. Once they made contact due to the imposed load, they could be lubricated by a free-standing film of *n*-pentanols trapped between them. The sliding process was simulated by applying external shear forces to mimic a constant shear stress, $\tau = F/A$, applied to each silicon atom on the outermost part of one layer, where F is the force applied in the sliding direction, parallel to the contact surface, distributed

uniformly among the outermost layer of silicon atoms, and A is the area of the contact surface within the simulation cell. The opposing layer experienced the same force but with an opposite direction (Fig. 2). To maintain system stability, an external force was applied to mimic a normal load, resulting in a normal pressure, $P_N = L/A$, applied to each silicon atom on the outermost part of both layers, distributed uniformly among them. We expect that artifacts at the contact surface were minimized by applying the load and shear stress solely to the atoms in the outermost layers.

The interaction potential used for the silicon oxide surfaces was based on the optimized potential for liquid simulations using all atoms (OPLS-AA) [31], adapted by Lorenz et al. [30]. This potential has been successfully used in previous studies on the tribological properties of silica surfaces lubricated with an ionic liquid [32] and the frictional properties of silica surfaces coated with self-assembled layers of hydrocarbons, perfluorocarbons, alcoholic chains, and their mixtures [23, 33]. The OPLS-AA force field was also chosen for the *n*-pentanol molecules since it has been used in similar studies of fluid phases. The OPLS-AA potential has been used in studies of several primary, secondary, and tertiary alcohols [34]. Its performance has been compared with other potentials, showing good agreement with experimental data [35]. The expressions of the contributions to the potential energy and the parameters used in the simulation are provided in the Supplemental Information.

The simulations were conducted using the large-scale atomic/molecular massively parallel simulator [36], using the particle–particle particle-mesh algorithm in 2D for electrostatic interactions [37]. Lennard–Jones interactions were truncated using a 10 Å cutoff radius, no long-range corrections were applied, and geometric combination rules determined all cross-interactions. Periodic boundary conditions were used to simulate an infinite contact surface, and all systems were maintained at 300 K using the Nose–Hoover thermostat [38–40]. The motion equations were integrated using a multiple timestep algorithm [41] with small timesteps of 0.075 fs for bonded interactions, 0.15 fs for valence and dihedral angle interactions, and 0.30 fs for all intermolecular and 1–5 intramolecular interactions. These small timesteps prevent artifacts at the contact surface, particularly at large sliding velocities [23, 33, 42, 43].

In this study, for a fixed value of P_N, we conducted several simulations while varying τ. We started with a relatively large τ (half of P_N) to induce considerable interfacial slip and observe the resulting "equilibration" process to a stationary state. Then, we proceeded with additional simulations in which we reduced τ until no interlayer displacement was detected. Through this procedure, we aimed to identify the static friction coefficient value where Amonton's law of friction is valid [44], in microscopic [45] and macroscopic [46] contacts. By analyzing the "equilibration" dynamics and the regimes of the displacements (single-slip, multiple-slip, or continuous), we could obtain a comprehensive understanding of the fundamental frictional mechanisms that govern the behavior of these layered materials.

3 Results and Discussion

MD simulations were conducted to study the behavior of sliding silica layers passivated with hydroxyl groups and *n*-pentanol chains as lubricants under external load, a range of shear stresses, and isothermal conditions. During the simulation, the *n*-pentanol chains' hydroxyl groups moved toward the silica surfaces and formed hydrogen bonds with the surface hydroxyl groups. The mechanical sliding process resulted in the saturation of each silica surface with a monolayer of adsorbed *n*-pentanol molecules. The *n*-pentanol chains' terminal methyl groups were identified as the contact surface for friction and sliding due to their lower frictional forces than the hydrogen-bond forces between the surface and *n*-pentanol hydroxyl groups. A snapshot of the stationary state of the two silica surfaces under external forces in the normal and lateral directions is shown in Fig. 3.

An external force of 200 kcal/(mol Å) was applied in the normal direction to simulate a compressive load in the system, generating a P_N of 552.56 MPa on each surface ($A = 53.9 \times 46.7$ Å^2). In the first simulation, the applied shear stress on each layer of the system was $P_N/4 = 138.14$ MPa, applied in opposing directions to each layer, giving a total shear stress of $\tau = 2\ (P_N/4) = P_N/2 = 276.28$ MPa. After the *n*-pentanols were fully adsorbed onto the silica surface, the layers periodically underwent stick and slip events or continuous sliding, depending on the magnitude of τ. After an "equilibration period," the system reached a stationary state. The *n*-pentanol chains were not completely perpendicular to the surfaces and tilted because of the load (Fig. 3, left). While the silica layers and adsorbed *n*-pentanols were free to move in the lateral direction perpendicular to the sliding direction, they did not show any motion in that direction (Fig. 3, right).

During the simulation, the two silica layers slid in opposite directions, as indicated by the time profile of their center of mass positions (Fig. 4). Given the lateral periodicity of the system, the layers could slide indefinitely in the sliding direction. Initially, the layers moved rapidly because they were not in contact. However, they slowed down when they came into contact (~ 0.03 ns), moving at a slower rate for approximately 0.26 ns. Then, the layers' displacement accelerated, and a steady state was reached after 0.97 ns. The temporal profile of the layers' absolute displacement was divided into three periods (Fig. 5a), with slopes (speeds) that could be associated with their degree of *n*-pentanol molecule adsorption and ordering. The first and second periods were

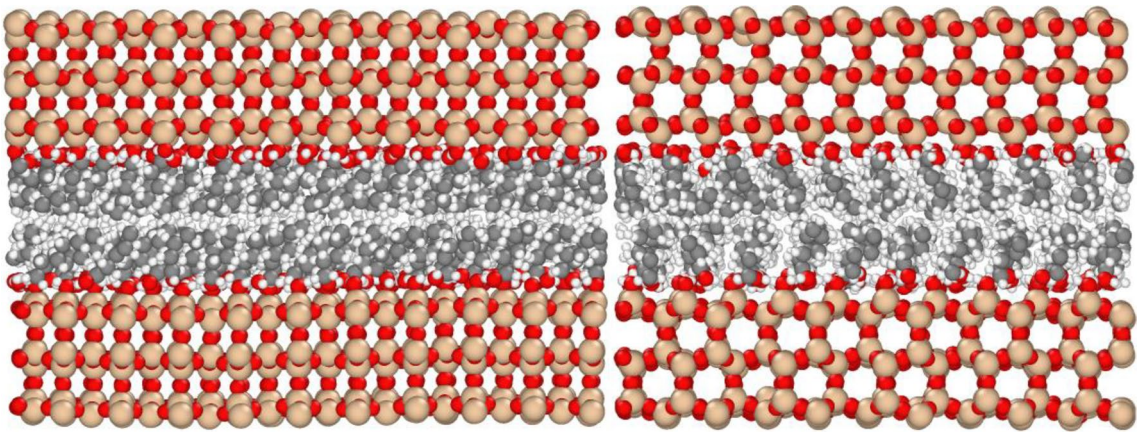

Fig. 3 Side views of silica (β-cristobalite) layers under *n*-pentanol lubrication. The outermost silicon atoms are exposed to uniformly distributed forces corresponding to $P_N = 552.56$ MPa and $\tau = ¼ P_N = 138.14$ MPa. The left image shows the sliding direction: the upper layer is sliding to the right, and the lower layer is sliding to the left. The right image shows the nonsliding direction. The observed tilt of the *n*-pentanol molecules is due to the normal load compressing the lubricant. The red, brown, gray, and white spheres represent oxygen, silicon, carbon, and hydrogen atoms, respectively

characterized as logarithmic growth and movement with constant acceleration, respectively. In contrast, the third period was characterized by a constant speed, expected in a stationary state. The slope changes clearly defined the time limit between the second and third periods. However, the time limit between the first and second periods was not evident in the profile.

The distribution of the *n*-pentanol chains' oxygen atoms between the two silica layers during the three periods is shown in the probability plots in Fig. 6a–c. The distributions

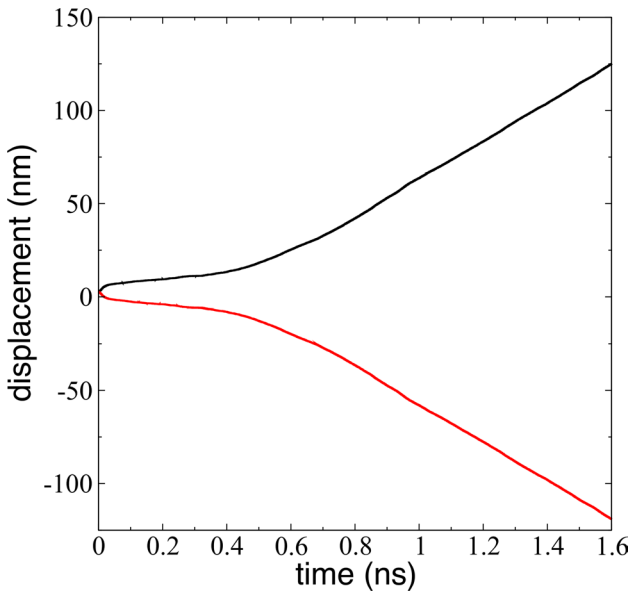

Fig. 4 Displacement of the center of mass of the upper (black) and lower (red) silica layers as a function of time. $P_N = 552.56$ MPa, $\tau = ½ P_N = 276.28$ MPa, and 300 K

were normal; they became narrower and taller as the simulation progressed toward the stationary state in period III. The number of unabsorbed lubricant molecules on the silica surfaces was quantified by integrating the probability profiles. Most *n*-pentanol chains adsorb onto the silica layers through hydrogen bonding with surface hydroxyls during the first 0.05 ns of period I, with an adsorption rate of 81%. The adsorption percentage increased during period I, reaching 86% in the final 0.05 ns. The adsorption fraction reached 88% within the first 0.05 ns of period II, where the absolute displacement accelerates constantly. Nearly all *n*-pentanol chains were adsorbed on the silica layers by the end of period II. In period III, the adsorption fraction remained full and constant. During period I, the unabsorbed hydroxyls of *n*-pentanols produced hydrogen-bond forces between lubricant molecules away from the silica surfaces, resulting in increased frictional forces between the layers and a low average velocity of 35.21 nm/ns. The full adsorption obtained in period II was likely due to the strong homogenizing force of the accelerated displacements, which constantly increased the speed of the layers.

The hydrogen bond network between the hydroxyl groups of the silica layers and lubricant molecules formed rapidly at the silica surfaces in period I. Figure 7a shows that most of the adsorbed *n*-pentanols' hydroxyl groups were evenly distributed and located between two surface hydroxyl groups, even in the early stages of the simulation (0.12 ns). The lubricant molecules' hydroxyl groups were oriented either between contiguous hydroxyl groups in the sliding direction or laterally contiguous groups forming a 30° angle with the sliding direction. Additionally, a few hydroxyl groups from *n*-pentanols formed small clusters during period I, which disappeared when the simulation entered

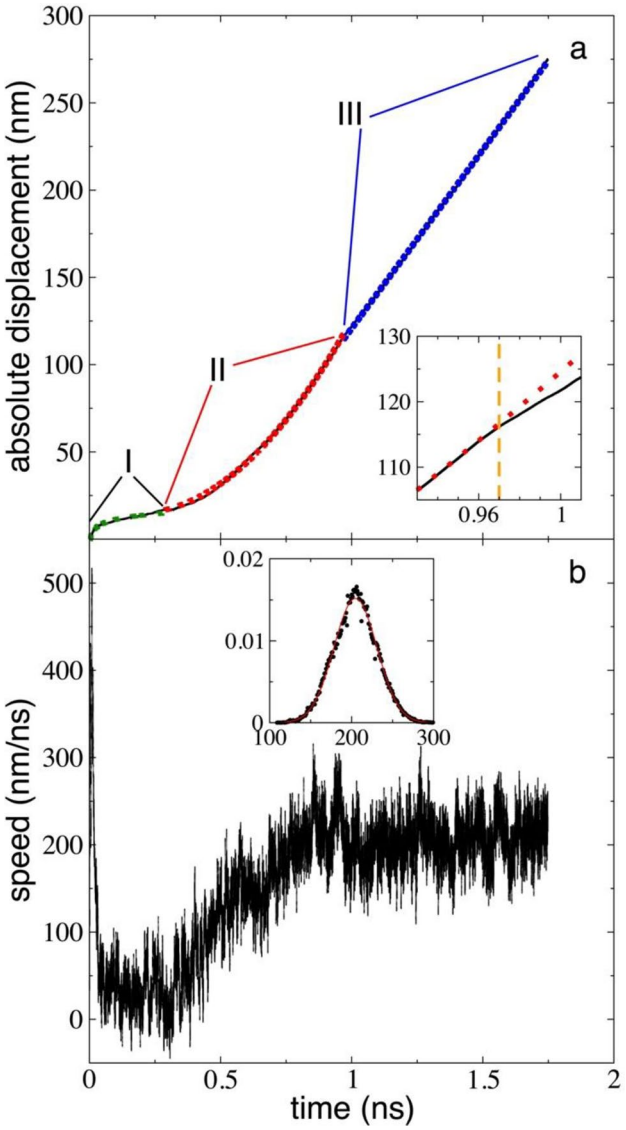

Fig. 5 **a** Absolute displacement and **b** speed of the silica layers as a function of time. P_N = 552.56 MPa, τ = ½ P_N = 276.28 MPa, and 300 K. The green dotted line in period I represents the fit to a natural logarithmic growth expression, $\{(3.438nm)ln[(266.631ns^{-1})t]\}$. The red dotted line in period II represents a quadratic fit (Eq. 1), while the blue dotted line in period III is a linear regression. Inset of (**a**): an expanded view of the transition time (~0.97 ns, dashed orange line) between periods II and III with the same axes and units as the original plot; black and red lines are the same as the original plot, and the red dotted line from period II was extrapolated beyond the transition time. Inset of (**b**): distribution of speeds for period III (speed units as in [**b**]); the red line represents a fit to the normal distribution function

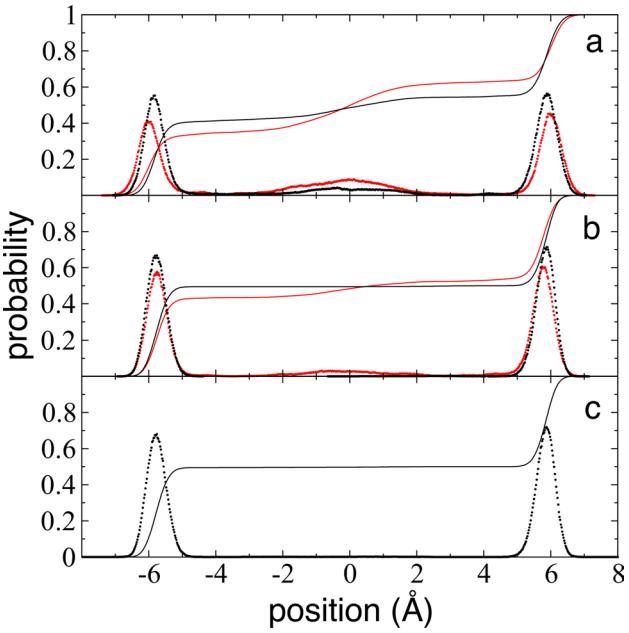

Fig. 6 Distribution of the *n*-pentanol molecules' oxygen atoms as a function of their position between the two silica layers at several periods during the simulation. **a** Beginning (0.03–0.08 ns, red dots) and end (0.24–0.29 ns, black dots) of period I in Fig. 5. **b** Beginning (0.29–0.34 ns, red dots) and end (0.92–0.97 ns, black dots) of period II in Fig. 5. **c** Beginning (0.97–1.02 ns, black dots) of period III in Fig. 5. Continuous lines are the integration of the corresponding probability distributions

the constant acceleration period (Fig. 7b). In the stationary state at constant velocity (Fig. 7c), the hydrogen bond distribution remained homogeneous. The lubricant molecules' hydroxyl groups continuously moved during the simulation. Instability events created by thermal fluctuations induced some hydroxyl groups to move from contiguous to laterally contiguous hydrogen bonds and vice versa, which is an energetically less expensive route than directly moving in the surface layer's sliding direction.

Figure 5a shows a detailed analysis of the displacements in period II. A quadratic expression corresponding to movement subject to constant acceleration was used to fit the data:

$$s(t) = s_0 + v_0(t - t_0) + \frac{1}{2}a_c(t - t_0)^2, \quad (1)$$

where s_0, v_0, and t_0 are the initial position, initial velocity, and time when period II begins, respectively, and a_c is the period's constant acceleration. These parameters were determined using subsets of data for period II, starting at different initial times but ending at the same time (0.97 ns), and choosing the data that matched the end speed of period II with the constant speed of period III (205 nm/ns). The constant acceleration in this period was calculated to be approximately 327.50 nm/ns^2, about 33.4 times the acceleration due to gravity. The rapid acceleration during the transition period (II) to the final stationary state at constant velocity (period III) was due to the high shear stress used, which was half the normal load. We confirmed the proposed displacement models for the three periods by calculating their speed profiles (Fig. 5b). They showed a rapid decrease in period I,

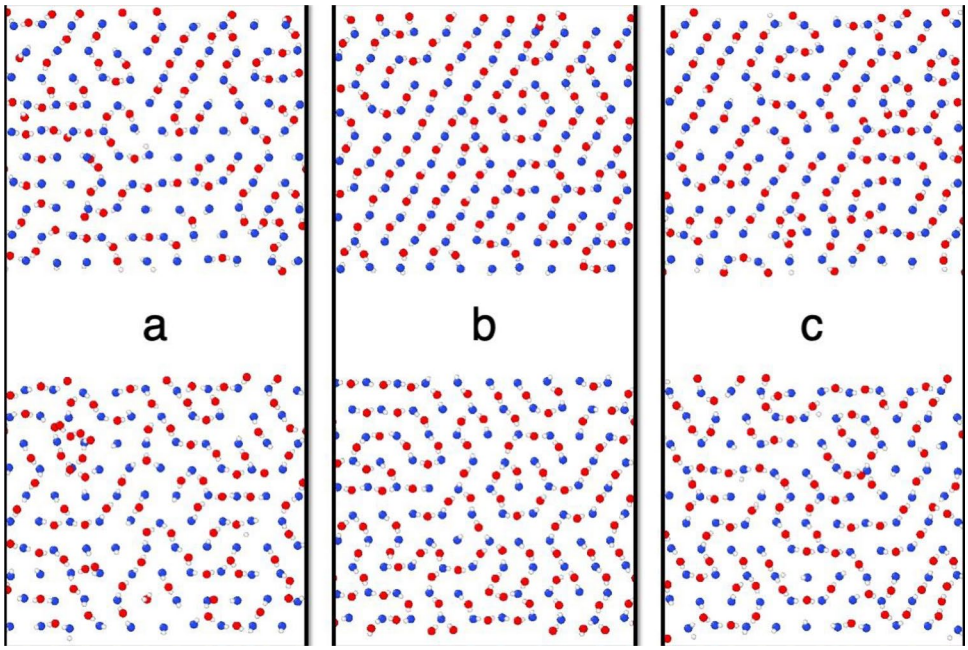

Fig. 7 Snapshots of the hydroxyl groups in the upper and lower silica layers (blue and white spheres represent oxygen and hydrogen, respectively) and the *n*-pentanol chains' hydroxyl groups (red and white spheres represent oxygen and hydrogen, respectively) at **a** 0.12 ns, **b** 0.29 ns, and **c** 0.97 ns. The upper layer slides to the right and the lower layer to the left under constant $P_N = 552.56$ MPa, constant $\tau = ½\ P_N = 276.28$ MPa, and 300 K

consistent with the natural logarithm growth expression used to model the absolute displacements. In the corresponding time interval in period II, the speed grew linearly, consistent with Eq. 1, and in period III, the speed remained constant, with large oscillations around a constant value. The speed distribution in period III was normal (Fig. 5b, inset) with a standard deviation of 26.31 nm/ns.

Several additional shear stresses were examined, ranging from 82.88 to 248.65 MPa, while keeping the normal load constant at 552.56 MPa at 300 K. At $\tau = 248.65$ MPa (0.45 P_N), a behavior similar to that seen at 276.28 MPa was observed, with the three distinct periods present (Fig. 8a). The initial transition state (period I) lasted twice as long as the period observed at $\tau = 276.28$ MPa (~2 ns), reaching a constant speed of 147.05 nm/ns in period III. A 10% reduction in shear stress resulted in a 29% reduction in the long-term speed. The analysis using Eq. 1 produced $v_0 = 1.21$ nm/ns and $a_c = 76.28$ nm/ns^2. The speed profile for periods I and III (Fig. 8b) showed a similar trend as that observed with $\tau = 276.28$ MPa. Speeds in period II showed periodic fluctuations, which were difficult to characterize as an incremental linear behavior (expected in an accelerated displacement). The speed profile for this period (II) comprised two regimes, one with small fluctuations and low positive and negative speeds (0.65–1.25 ns), followed by one with large positive fluctuations (1.25–2.00 ns). Together, they result in positive displacements with a quadratic behavior like that observed with $\tau = 276.28$ MPa in the same period (Fig. 5a). The speed distribution for period III showed large deviations from the normal distribution (Fig. 8b, inset), with a standard deviation of 20.51 nm/ns.

Further reducing τ increased the duration of period I and decreased the constant speed of period III (Fig. 9a). At $\tau = 221.02$ MPa, period I extended to 2.6 ns, and the constant speed for period III decreased to 52.97 nm/ns. At this τ, the first stick events between long continuous sliding (Fig. 9a, inset plots) occurred in period III, lasting ~ 0.02 ns, which are probably due to temporary conformations with higher cohesivity [47–49]. Simulations under a forced constant speed (at the same tribological conditions) are expected to show more periodic stick and slip behavior due to periodic lapses where conformations can reorganize [23, 33, 50, 51]. The speed profile (Fig. 9b) for period I showed a rapid decay to a subperiod of small fluctuations around zero, which lasted the rest of period I. The behavior of period II was like that observed for $\tau = 248.65$ MPa, comprising two subperiods with small and large fluctuations, respectively, but the period of large fluctuations showed variations in speed like those observed in period III. Period III showed large fluctuations but with a bimodal distribution (inset of Fig. 9b), with one peak around zero and the other around 77 nm/ns, 50% higher than the average speed for this period. This bimodal speed distribution reflects the first developments of stick events.

Additional reductions in τ increased the frequency of adhesion periods, with the lowest net displacement achieved at $\tau = 110.51$ MPa (0.20 P_N). In this regime, the layers remained adhered but slid over each other for short periods, indicating a single-slip behavior (Fig. 10a). The slides had a constant displacement (~ 0.27 nm), equivalent to half the separation between two surface hydroxyl groups in the sliding direction. This observation suggests that two slip types occurred: one that brought the terminal methyl

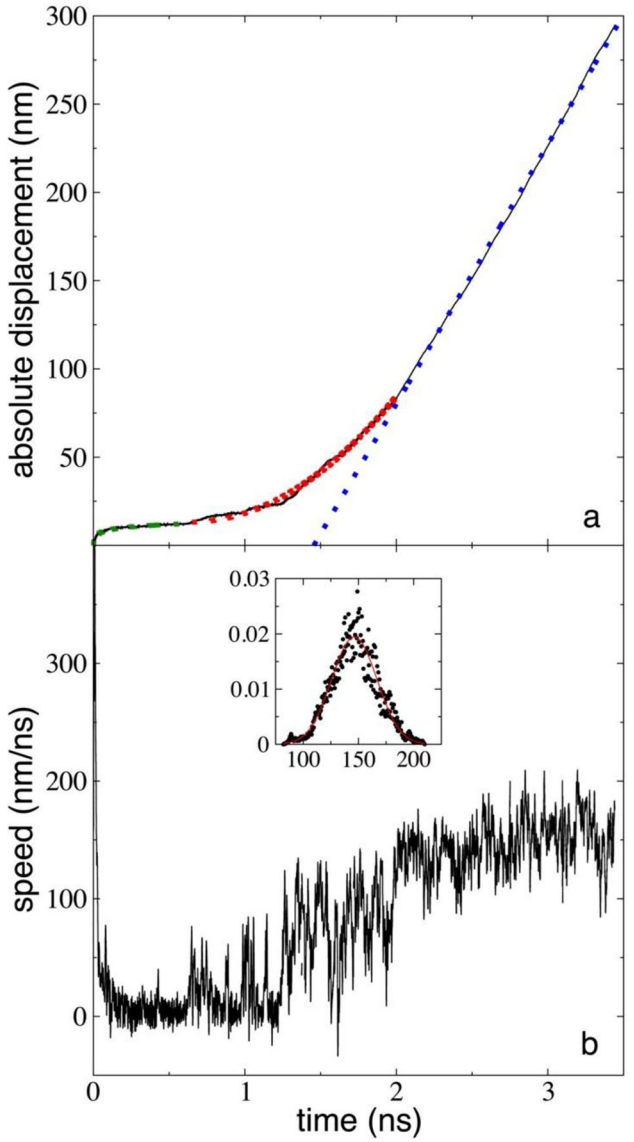

Fig. 8 **a** Absolute displacement and **b** speed of the silica layers as a function of time. $P_N = 552.56$ MPa, $\tau = 45\%$ $P_N = 248.65$ MPa, and 300 K. The green dotted line in period I represents the fit to a natural logarithmic growth expression, $\{(1.961nm)ln[(853.957ns^{-1})t]\}$. The red dotted line in period II represents a quadratic fit (Eq. 1), while the blue dotted line in period III is a linear regression. Inset of (b): distribution of speed values for period III (speed units as in [b]); the red line represents a fit to the normal distribution function

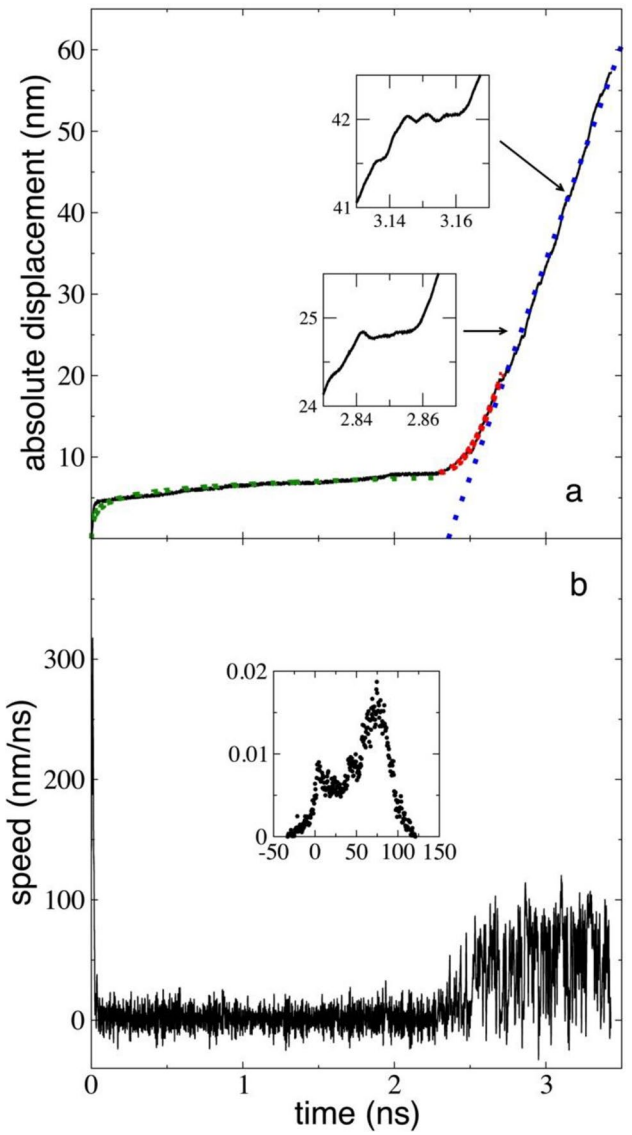

Fig. 9 **a** Absolute displacement and **b** speed of the silica layers as a function of time. $P_N = 552.56$ MPa, constant $\tau = 40\%$ $P_N = 221.02$ MPa, and 300 K. The green dotted line in period I represents a fit to a natural logarithmic growth expression $\{(1.015nm)ln[(685.009ns^{-1})t]\}$. The red dotted line in period II represents a quadratic fit (Eq. 1), while the blue dotted line in period III is a linear regression. Insets of (a): expanded views of the stick and slip events with the same axes and units as the original plot; the black lines are the same as the original plot. Inset of (b): distribution of speed values for period III (speed units as in [b])

groups from the lubricant chains in the sliding direction into contact, followed by a second type that separated them and brought lubricant chains located laterally contiguous into contact. When the chains in the sliding direction are in contact, the laterally contiguous separate, and vice versa. The long intervals (few ns) between slips were necessary for the chains' end groups to pass and laterally surround each other. Due to computational limitations, the simulation profile for $\tau = 110.51$ MPa does not start at time zero, with the initial state coming from higher τ simulations (period III). At this τ, the adhesion periods were longer than the slip periods, indicating a single-slip regime. This behavior contrasts with those at higher shear stresses, where multiple slips (and single slips) were present; at even higher shear stresses, adhesion periods disappeared (smooth and continuous sliding) [20]. A linear regression analysis showed a very low speed of approximately 0.128 nm/ns. The speed profile showed

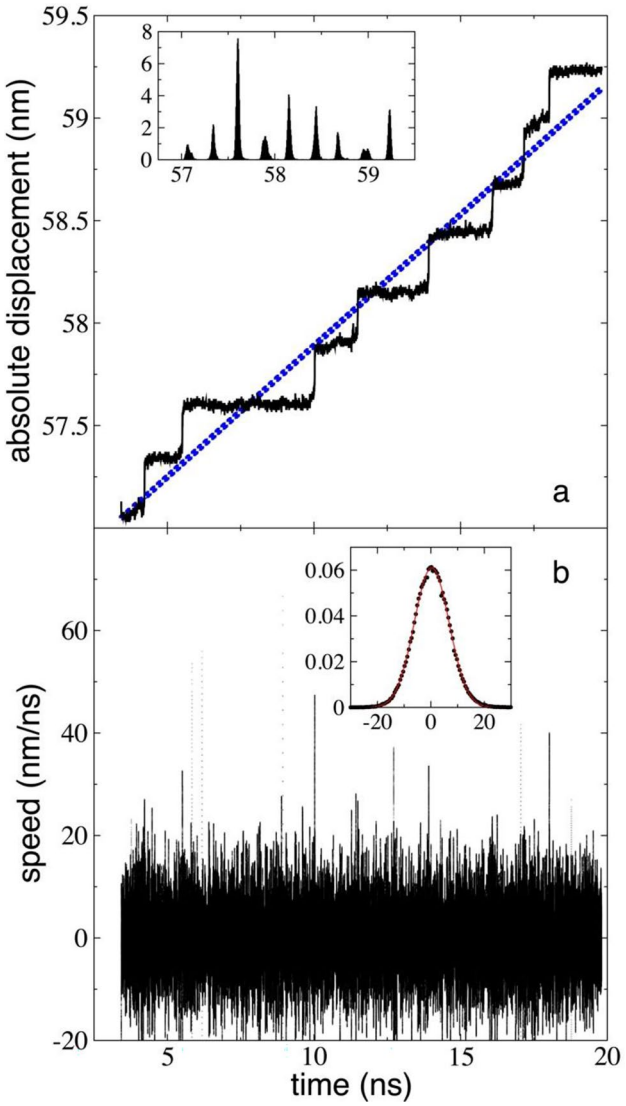

Fig. 10 **a** Absolute displacement and **b** speed of the silica layers as a function of time. $P_N = 552.56$ MPa, $\tau = 20\%$ $P_N = 110.51$ MPa, and 300 K. The blue dotted line is a linear regression. Inset of (**a**): probability distribution of the absolute displacements (units of displacements same as in [**a**]). Inset of (**b**): distribution of speed values for period III (speed units as in [**b**]); the red line represents a fit to the normal distribution function

large and uniform fluctuations (Fig. 10b), translating into a normal distribution (Fig. 10b, inset) with a standard deviation of 6.53 nm/ns. The fast slip displacements occurred almost instantly. Therefore, the number of events occurring at high speeds is greatly reduced and undetectable in the speed distribution.

At the lowest τ used in this study (82.88 MPa, 0.15 P_N), the layers moved slowly in the same direction and remained adhered, unlike at higher shear stresses where each layer moved in the direction of the applied τ. This observation indicates that the minimum τ required to overcome the static

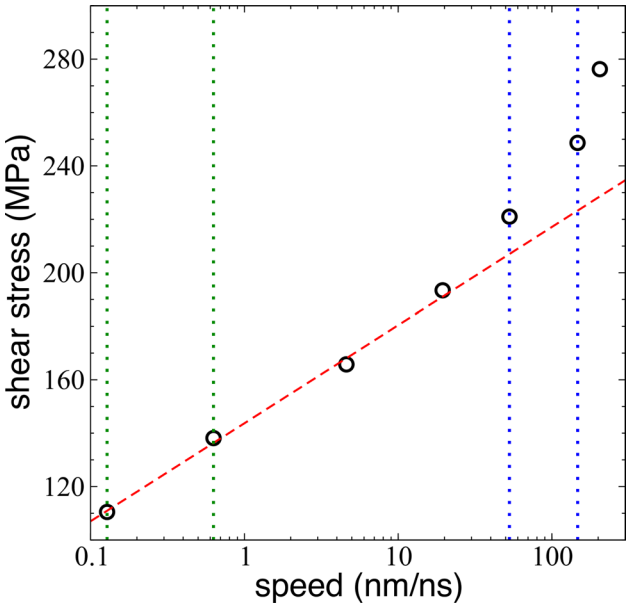

Fig. 11 Shear stress as a function of the speed of the absolute displacement. $P_N = 552.56$ MPa and 300 K. Inset: logarithmic dependence of shear stress on the logarithm of the speed. The red line represents a linear regression using the lowest four shear stresses. Green dotted lines represent the transition region from single to multiple slips. Blue dotted lines represent the transition region to continuous sliding (Color figure online)

frictional forces between the layers is between 15 and 20% of P_N (552.56 MPa), corresponding to the static coefficient of friction (μ_s), which ranged between 0.15 and 0.20. Similar behavior has been observed experimentally, with μ_s values between 0.15 [2] and 0.20 [52] obtained when studying the rotation of borosilicate balls on quartz surfaces lubricated with *n*-pentanol at a $P_N = 199$ MPa, room temperature, and speeds between 0.11 and 0.33 m/s.

Figure 11 shows the correlation between the studied τ values, and the stationary speeds obtained in the simulations based on absolute displacements between the layers. Previous sliding contact experiments using steel at 540 °C and vapor phase lubrication with acetylene also showed a similar relationship between shear stress and speed [53]; the experimental results followed a logarithmic pattern and were consistent with the Prandtl–Tomlinson thermal (PTT) model [54–56] specific to single-slip displacements [57–59]. The average velocities obtained in this study at fixed shear stresses were significantly higher than those in experimental studies on tribological devices and atomic force microscopy experiments but similar to the sliding conditions of the moving parts of NEMs [1].

In the PTT model, low shear stress values and the corresponding logarithm of their speed followed a linear behavior up to a characteristic speed (v_a), representing the limit speed at which thermal energy aids single slip events and above which frictional forces approach a plateau [55]. Based on the

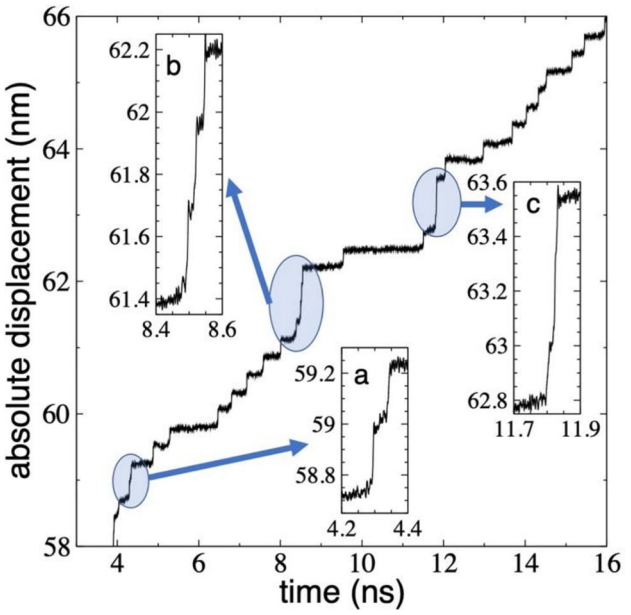

Fig. 12 Absolute displacement of the silica layers as a function of time. $P_N = 552.56$ MPa, $\tau = 25\%$ $P_N = 138.14$ MPa, and 300 K. Insets: Expanded views of the stick and slip events with the same axes and units as the original plot. **a** Two single slips. **b** Three single slips. **c** One single slip followed by one double slip

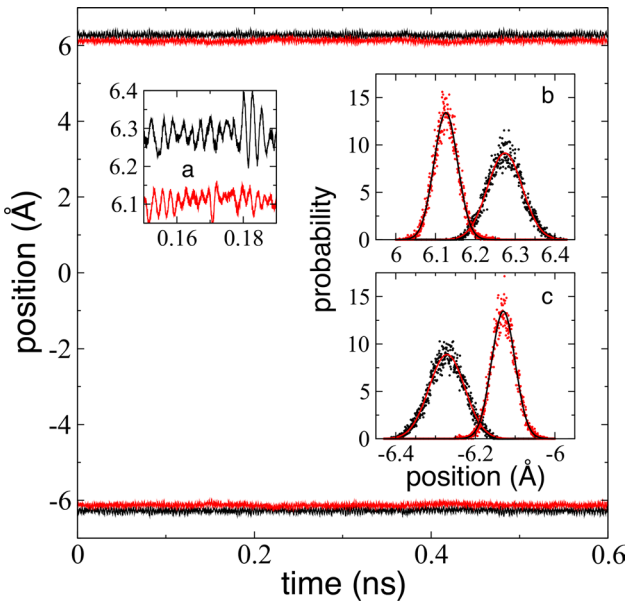

Fig. 13 Temporal profile of the average position of the oxygen atoms in the hydroxyl groups passivating the silica layers at constant $P_N = 552.56$ MPa and 300 K in the constant velocity regime. Black points represent continuous sliding behavior at $\tau = 50\%$ $P_N = 276.28$ MPa (period III), and red points represent single slip sliding behavior at $\tau = 20\%$ $P_N = 110.51$ MPa. Insets: **a** Expanded view of the temporal profiles with the same axes and units as the original plot; **b–c** Black and red points are the probability distributions of the corresponding temporal profiles of the oxygen positions. Continuous lines represent fits to normal distributions (Color figure online)

three lowest shear stresses and their corresponding speeds in this study, the linear regression of shear stress on the logarithm of speed found that v_a was at ~ 20 nm/ns, well into the region where single- and multiple-slip events occur. In this study, speeds beyond v_a are in the transition region towards continuous sliding behavior, where additional increments in τ are not proportional to the logarithm of the speed obtained, likely due to some additional energy loss mechanism with the surroundings present at these high speeds. Similar results for v_a have been reported for simulations of Pt tips sliding on Au surfaces [59]. The v_a value in Pt/Au simulations was higher than that observed in corresponding atomic force microscopy experiments, possibly due to the simulations' failure to accurately replicate the experimental cantilever's mechanical response [59]. The same issue may also affect this study's results due to the small thickness and area of the simulated layers. Comparable experimental results using high speeds are challenging due to technical difficulties, resulting in unwanted resonant frequencies that affect the accuracy of measured tribological properties [60]. The oscillation frequency naturally occurring in shear stresses and normal loads of constant-speed experiments is especially impacted by the equipment's resonant frequencies.

Figure 12 shows the multiple-slip regime at $\tau = 238.1$ MPa (0.25 P_N) and 300 K, where multiple slips result from several single slips occurring after short stick periods (~ 0.02 ns). Some are genuinely multiple slips, following single slips and long stick events. Multiple slips are not continuous but infrequent events that occur after a sequence of single slip events. Due to the presence of long stick and very short slip periods, the speed profile is expected to be very similar to that observed with $\tau = 110.51$ MPa, where the high speeds due to slip events are undetectable in the speed distribution.

We analyzed the atomic position distribution of oxygen atoms in the silica surfaces along the normal axis to the surfaces, comparing systems under the smallest (20% P_N) and largest (50% P_N) τ conditions, representing single-slip and continuous sliding regimes, respectively. Figure 13 shows the temporal profiles of the average position of oxygen atoms in the hydroxyl groups on the silica surface (averaged for all oxygen atoms in each surface layer). Compared to the lowest τ system, the highest τ system showed a slight expansion in the normal direction (~ 0.58 Å), representing the volume increment occupied by the lubricant. The increase corresponds to half the van der Waals radius of a hydrogen atom (1.20 Å) [61] and translates into an increased *n*-pentanol molecular volume of ~ 7.30 $Å^3$, sufficient to accommodate a single hydrogen atom's van der Waals volume. However, due to the *n*-pentanol chains' compact localization and orientation, the additional volume is created in the normal direction. The additional space gives hydroxyl or methyl groups more freedom to move, not only in the normal and sliding

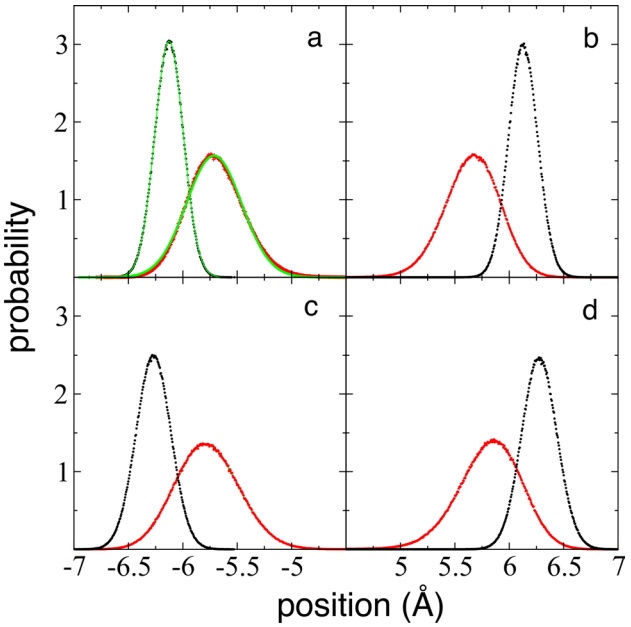

Fig. 14 Probability distributions of the positions of the oxygen atoms along the normal direction to the (111) plane of the silica layers at constant $P_N = 552.56$ MPa and 300 K. The position of 0 Å represents the center of the simulation box. Black and red points represent oxygens from the hydroxyl groups of the silica layer and the *n*-pentanol chains, respectively. Results using $\tau = 50\%$ $P_N = 276.28$ MPa are shown for the **a** lower and **b** upper layers. Results using $\tau = 20\%$ $P_N = 110.51$ MPa are shown for the **c** lower and **d** upper layers. Continuous green lines represent fits to normal distributions (Color figure online)

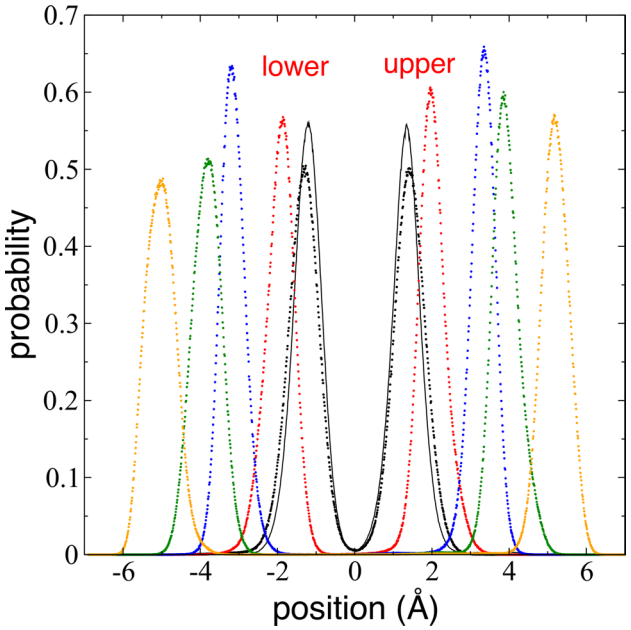

Fig. 15 Probability distributions of the position of the carbon atoms along the normal direction to the (111) plane of the silica layers at constant $P_N = 552.56$ MPa and 300 K. Results using $\tau = 50\%$ $P_N = 276.28$ MPa are shown as dotted lines. Results using $\tau = 25\%$ $P_N = 110.51$ MPa are shown as solid black lines. Given the formula for *n*-pentanol (C^aH_3–C^bH_2–C^cH_2–C^dH_2–C^eH_2–OH), black, red, blue, green, and orange lines represent the distributions of the carbon atoms C^a, C^b, C^c, C^d, and C^e, respectively (Color figure online)

directions but also in the lateral direction, facilitating the sliding of the layers [23].

The temporal profiles of average positions indicated a breathing behavior for the layers (Fig. 13a), visible as small oscillations of up to 0.2 Å. These oscillations, with periods of approximately 3.2 ps, were not due to slipping events. The probability distributions of these oscillations were normal (Fig. 13b and c), and the distribution widened for the profile corresponding to the continuous sliding regime using the largest τ. The normal distribution of separations indicates that using constant force to control the load in simulations produces reliable results that may not be obtained with constant-separation simulations [13]. These oscillations represent expansions and contractions naturally present in any solid [62] or nanostructure [63]. Their normal distribution suggests that the external forces imposed on the outermost layer of silicon atoms do not create artifacts in the mechanical behavior of the layers under shear stress.

Figure 14a–d show the probability distributions of oxygen positions for hydroxyl groups in the silica surface and *n*-pentanol chains using the smallest (20% P_N) and largest (50% P_N) τ conditions. The distributions for *n*-pentanol chains were shorter and wider than those for the surface hydroxyl groups, indicating greater freedom of movement in the normal direction for the lubricant's hydroxyl groups. The average separation between the means of both distributions (surface and chains) did not differ between the smallest and largest τ conditions, indicating that hydrogen bond forces dominate interactions between hydroxyl groups and that the shear forces transmitted to hydroxyl groups at the contact surface are insufficient to affect the hydrogen bond network.

Upon adsorption of the lubricant chains onto the silica surfaces, upper and lower monolayers formed, with sliding occurring at the contact surface formed by their methyl groups. The probabilities of the positions in the normal direction of the *n*-pentanol chains' methyl groups at the active contact surface were normally distributed (Fig. 15). The mean separation of the upper and lower lubricant chain monolayers was approximately 2.54 Å with the smallest (20% P_N) τ and approximately 2.70 Å with the largest (50% P_N) τ, reflecting an increase in separation of only 0.14 Å, which is a fraction of the total lubricant expansion. The means for the other carbons are also plotted for the largest τ condition in Fig. 15, with the means for the methyl carbon and the next bonded methylene carbon being very close, with a difference of only 0.55 Å. The *n*-pentanol chains' zigzag conformation led to similar carbon separations for the next two methylene groups in the chain. This conformation

results from the chains' degree of tilting relative to the silica surfaces.

4 Conclusions

MD simulations were performed for silica surfaces passivated with hydroxyl groups to anchor *n*-pentanol chains as a lubricant, which formed two adsorbed monolayers under isothermal and constant load and shear stress conditions. At a normal pressure of 552.56 MPa and 300 K, three regimes were identified for shear stresses between 20 and 50% of the normal pressure: single slips, multiple slips (in association with single slip events), and continuous sliding.

Single slips occurred at constant displacements of 0.27 Å, which is half the separation between two surface hydroxyls in the sliding direction, indicating a two-step process. The two-step process is the result of the location of the lubricant hydroxyls on the silica surface, which can be either between two contiguous surface hydroxyls in the sliding direction, or laterally contiguous forming a 30° angle. Laterally contiguous are as numerous as those contiguous in the sliding direction and are located half the separation between two surface hydroxyls in the sliding direction.

Multiple slips occurred at shear stresses between 25 and 40% of the normal pressure and can occur after short sticking periods. Continuous sliding occurred at shear stresses between 45 and 50% of the normal pressure, reaching accelerations up to 34 times that of gravity in the periods before reaching the stationary state. The stationary state of constant speed is reached when all the lubricant molecules form homogeneously distributed hydrogen bonds with hydroxyl groups at the silica surfaces. For large shear rates, the periods before reaching the stationary state can be modeled as natural logarithm growth followed by displacements at constant accelerations. In the range of studied stresses, the lubricant volume increased with increasing shear stress, resulting in an expansion of 0.58 Å in the normal direction or 7.30 $Å^3$ per *n*-pentanol chain when the lowest and highest shear stresses studied in this work are compared. This lubricant expansion is achieved by larger separations between interlayer methyl-methyl contacts and by lowering the *n*-pentanol chains' tilting angles.

The stationary states' speed profiles showed normal distributions for the smallest (single slip events) and largest (continuous sliding) shear stresses examined in this study. For intermediate shear stresses, the distributions range from near-normal to bimodal distributions, with one of the peaks at zero, corresponding to stick events.

Supplementary Information The online version contains supplementary material available at https://doi.org/10.1007/s11249-023-01731-6.

Author Contributions All authors contributed to the study conception and design. Material preparation, data collection and analysis were performed by JLR, VMB-S, RG-G, FIR-Z, and EL. The first draft of the manuscript was written by JLR and all authors commented on previous versions of the manuscript. All authors read and approved the final manuscript.

Funding This work was supported by CONACYT (México) through an infrastructure fellowship (Grant number 268652), and the Universidad Michoacana de San Nicolás de Hidalgo through research funds under the CIC program.

Declarations

Conflict of interest The authors have no relevant financial or non-financial interests to disclose.

References

1. Kim, S.H., Asay, D.B., Dugger, M.T.: Nanotribology and MEMS. Nano Today **2**, 22–29 (2007). https://doi.org/10.1016/S1748-0132(07)70140-8
2. Asay, D.B., Dugger, M.T., Kim, S.H.: In-situ vapor-phase lubrication of MEMS. Tribol. Lett. **29**, 67–74 (2008). https://doi.org/10.1007/s11249-007-9283-0
3. He, X., Liu, Z., Ripley, L.B., Swensen, V.L., Griffin-Wiesner, I.J., Gulner, B.R., McAndrews, G.R., Wieser, R.J., Borovsky, B.P., Wang, Q.J., et al.: Empirical relationship between interfacial shear stress and contact pressure in micro- and macro-scale friction. Tribol. Int. **155**, 106780 (2021). https://doi.org/10.1016/j.triboint.2020.106780
4. Khomenko, A., Boyko, D., Khomenko, K.: Atomistic tribological investigation of ultrathin layer of carbon disulfide between diamond surfaces. Mol. Cryst. Liq. Cryst. **719**, 1–10 (2021). https://doi.org/10.1080/15421406.2020.1860531
5. Khomenko, A.V., Boyko, D.V., Zakharov, M.V.: Molecular dynamics of a thin liquid argon layer squeezed between diamond surfaces with a periodic relief. J. Frict. Wear **39**, 152–157 (2018). https://doi.org/10.3103/S106836661802006X
6. Khomenko, A.V., Lyashenko, I.A., Borisyuk, V.N.: Multifractal analysis of stress time series during ultrathin lubricant film melting. Fluct. Noise Lett. **09**, 19–35 (2010). https://doi.org/10.1142/S0219477510000046
7. Gao, S., Yang, L.H., Gan, Y., Chen, Q.: The influence of sliding speed on the friction behavior of silica surface. ACS Omega **6**, 3384–3389 (2021). https://doi.org/10.1021/acsomega.0c05897
8. Li, C., Tang, W., Tang, X.-Z., Yang, L., Bai, L.: A molecular dynamics study on the synergistic lubrication mechanisms of graphene/water-based lubricant systems. Tribol. Int. **167**, 107356 (2022). https://doi.org/10.1016/j.triboint.2021.107356
9. de Beer, S., Kenmoé, G.D., Müser, M.H.: On the friction and adhesion hysteresis between polymer brushes attached to curved surfaces: rate and solvation effects. Friction **3**, 148–160 (2015). https://doi.org/10.1007/s40544-015-0078-2
10. Hu, C., Yi, C., Bai, M., Lv, J., Tang, D.: Molecular dynamics study of the frictional properties of multilayer MoS2. RSC Adv. **10**, 17418–17426 (2020). https://doi.org/10.1039/D0RA00995D
11. Pan, L., Yu, H., Lu, S., Lin, G.: Effects of surface nanostructure on boundary lubrication using molecular dynamics. Nanotechnol. Precis. Eng. **4**, 33005 (2021). https://doi.org/10.1063/10.0005222
12. Zhou, Y., Huang, Y., Li, J., Zhu, F.: Effect of water film on the nano-scratching process of 4H-SiC under the constant load.

Tribol. Int. **175**, 107802 (2022). https://doi.org/10.1016/j.triboint.2022.107802
13. Gattinoni, C., Maćkowiak, S., Heyes, D.M., Brańka, A.C., Dini, D.: Boundary-controlled barostats for slab geometries in molecular dynamics simulations. Phys. Rev. E **90**, 43302 (2014). https://doi.org/10.1103/PhysRevE.90.043302
14. Manzato, C., Foster, A.S., Alava, M.J., Laurson, L.: Friction control with nematic lubricants via external fields. Phys. Rev. E **91**, 12504 (2015). https://doi.org/10.1103/PhysRevE.91.012504
15. Chen, S., Guo, Z., Zhang, H., Pagonabarraga, I., Zhang, X.: Maximizing friction by liquid flow clogging in confinement. Eur. Phys. J. E **45**, 60 (2022). https://doi.org/10.1140/epje/s10189-022-00208-z
16. Hou, Y., Zhang, H., Wu, J., Wang, L., Xiong, H.: Study on the microscopic friction between tire and asphalt pavement based on molecular dynamics simulation. Int. J. Pavement Res. Technol. **11**, 205–212 (2018). https://doi.org/10.1016/j.ijprt.2017.09.001
17. Cui, S.T., Cummings, P.T., Cochran, H.D.: Molecular simulation of the transition from liquidlike to solidlike behavior in complex fluids confined to nanoscale gaps. J. Chem. Phys. **114**, 7189–7195 (2001). https://doi.org/10.1063/1.1359736
18. Carrillo, J.-M.Y., Russano, D., Dobrynin, A.V.: Friction between brush layers of charged and neutral bottle-brush macromolecules. Molecular dynamics simulations. Langmuir **27**, 14599–14608 (2011). https://doi.org/10.1021/la203525r
19. Brinkmann, K., Teichler, H.: Flow state in molecular-dynamics-simulated deformed amorphous ${\mathrm{Ni}}_{0.5}{\mathrm{Zr}}_{0.5}$. Phys. Rev. B. **66**, 184205 (2002). https://doi.org/10.1103/PhysRevB.66.184205
20. Medyanik, S.N., Liu, W.K., Sung, I.-H., Carpick, R.W.: Predictions and observations of multiple slip modes in atomic-scale friction. Phys. Rev. Lett. **97**, 136106 (2006). https://doi.org/10.1103/PhysRevLett.97.136106
21. Krylov, S.Y., Frenken, J.W.M.: The physics of atomic-scale friction: Basic considerations and open questions. Phys. status solidi **251**, 711–736 (2014). https://doi.org/10.1002/pssb.201350154
22. Wang, Z.-J., Ma, T.-B., Hu, Y.-Z., Xu, L., Wang, H.: Energy dissipation of atomic-scale friction based on one-dimensional Prandtl–Tomlinson model. Friction **3**, 170–182 (2015). https://doi.org/10.1007/s40544-015-0086-2
23. Rivera, J.L., Jennings, G.K., McCabe, C.: Examining the frictional forces between mixed hydrophobic-Hydrophilic alkylsilane monolayers. J. Chem. Phys. **136**, 244701 (2012). https://doi.org/10.1063/1.4729312
24. Scandella, L., Meyer, E., Howald, L., Lüthi, R., Guggisberg, M., Gobrecht, J., Güntherodt, H.-J.: Friction forces on hydrogen passivated (110) silicon and silicon dioxide studied by scanning force microscopy. J. Vac. Sci. Technol. B Microelectron. Nanom. Struct. Process. Meas. Phenom. **14**, 1255–1258 (1996). https://doi.org/10.1116/1.588526
25. Tsagkaropoulou, G., Warrens, C.P., Camp, P.J.: Interactions between friction modifiers and dispersants in lubricants: the case of glycerol monooleate and polyisobutylsuccinimide-polyamine. ACS Appl. Mater. Interfaces **11**, 28359–28369 (2019). https://doi.org/10.1021/acsami.9b05718
26. Greenfield, M.L., Ohtani, H.: Friction and normal forces of model friction modifier additives in simulations of boundary lubrication. Mol. Phys. **117**, 3871–3883 (2019). https://doi.org/10.1080/00268976.2019.1670876
27. Apóstolo, R.F.G., Tsagkaropoulou, G., Camp, P.J.: Molecular adsorption, self-assembly, and friction in lubricants. J. Mol. Liq. **277**, 606–612 (2019). https://doi.org/10.1016/j.molliq.2018.12.099
28. Rozanska, X., Delbecq, F., Sautet, P.: Reconstruction and stability of β-cristobalite 001, 101, and 111 surfaces during dehydroxylation. Phys. Chem. Chem. Phys. **12**, 14930–14940 (2010). https://doi.org/10.1039/C0CP00287A
29. Zhuravlev, L.T.: The surface chemistry of amorphous silica. Zhuravlev model. Colloids Surf. A Physicochem. Eng. Asp. **173**, 1–38 (2000). https://doi.org/10.1016/S0927-7757(00)00556-2
30. Lorenz, C.D., Webb, E.B., Stevens, M.J., Chandross, M., Grest, G.S.: Frictional dynamics of perfluorinated self-assembled monolayers on amorphous SiO2. Tribol. Lett. **19**, 93–98 (2005). https://doi.org/10.1007/S11249-005-5085-4
31. Jorgensen, W.L., Madura, J.D., Swenson, C.J.: Optimized intermolecular potential functions for liquid hydrocarbons. J. Am. Chem. Soc. **106**, 6638–6646 (1984). https://doi.org/10.1021/ja00334a030
32. Cione, A.M., Mazyar, O.A., Booth, B.D., McCabe, C., Jennings, G.K.: Deposition and wettability of [bmim][triflate] on self-assembled monolayers. J. Phys. Chem. C **113**, 2384–2392 (2009). https://doi.org/10.1021/jp808098w
33. Lewis, J.B., Vilt, S.G., Rivera, J.L., Jennings, G.K., McCabe, C.: Frictional properties of mixed fluorocarbon/hydrocarbon silane monolayers: a simulation study. Langmuir **28**, 14218–14226 (2012). https://doi.org/10.1021/la3024315
34. Stephenson, S.K., Offeman, R.D., Robertson, G.H., Orts, W.J.: Hydrogen-bond networks in linear, branched and tertiary alcohols. Chem. Eng. Sci. **62**, 3019–3031 (2007). https://doi.org/10.1016/j.ces.2007.03.007
35. Jorge, M., Gulaboski, R., Pereira, C.M., Cordeiro, M.N.D.S.: Molecular dynamics study of 2-nitrophenyl octyl ether and nitrobenzene. J. Phys. Chem. B **110**, 12530–12538 (2006). https://doi.org/10.1021/JP061301J
36. Plimpton, S.: Fast parallel algorithms for short-range molecular-dynamics. J. Comput. Phys. **117**, 1–19 (1995). https://doi.org/10.1006/jcph.1995.1039
37. Crozier, P.S., Rowley, R.L., Henderson, D.: Molecular-dynamics simulations of ion size effects on the fluid structure of aqueous electrolyte systems between charged model electrodes. J. Chem. Phys. **114**, 7513–7517 (2001). https://doi.org/10.1063/1.1362290
38. Nosé, S.: A unified formulation of the constant temperature molecular dynamics methods. J. Chem. Phys. **81**, 511 (1984). https://doi.org/10.1063/1.447334
39. Nosé, S.: A molecular dynamics method for simulations in the canonical ensemble. Mol. Phys. **52**, 255–268 (1984). https://doi.org/10.1080/00268978400101201
40. Hoover, W.G.: Canonical dynamics: equilibrium phase-space distributions. Phys. Rev. A **31**, 1695–1697 (1985). https://doi.org/10.1103/PhysRevA.31.1695
41. Tuckerman, M., Berne, B.J., Martyna, G.J.: Reversible multiple time scale molecular dynamics. J. Chem. Phys. **97**, 1990–2001 (1992). https://doi.org/10.1063/1.463137
42. Booth, B.D., Vilt, S.G., Lewis, J.B., Rivera, J.L., Buehler, E.A., McCabe, C., Jennings, G.K.: Tribological durability of silane monolayers on silicon. Langmuir (2011). https://doi.org/10.1021/la104778q
43. Reißer, S., Poger, D., Stroet, M., Mark, A.E.: Real cost of speed: the effect of a time-saving multiple-time-stepping algorithm on the accuracy of molecular dynamics simulations. J. Chem. Theory Comput. **13**, 2367–2372 (2017). https://doi.org/10.1021/acs.jctc.7b00178
44. Müser, M.H., Wenning, L., Robbins, M.O.: Simple microscopic theory of Amontons's laws for static friction. Phys. Rev. Lett. **86**, 1295–1298 (2001). https://doi.org/10.1103/PhysRevLett.86.1295
45. Homola, A.M., Israelachvili, J.N., McGuiggan, P.M., Gee, M.L.: Fundamental experimental studies in tribology: the transition from "interfacial" friction of undamaged molecularly smooth surfaces to "normal" friction with wear. Wear **136**, 65–83 (1990). https://doi.org/10.1016/0043-1648(90)90072-I

46. Popov, V.L., Li, Q., Lyashenko, I.A., Pohrt, R.: Adhesion and friction in hard and soft contacts: theory and experiment. Friction **9**, 1688–1706 (2021). https://doi.org/10.1007/s40544-020-0482-0
47. Socoliuc, A., Bennewitz, R., Gnecco, E., Meyer, E.: Transition from stick-slip to continuous sliding in atomic friction: entering a new regime of ultralow friction. Phys. Rev. Lett. **92**, 134301 (2004). https://doi.org/10.1103/PhysRevLett.92.134301
48. Tonazzi, D., Massi, F., Baillet, L., Culla, A., Di Bartolomeo, M., Berthier, Y.: Experimental and numerical analysis of frictional contact scenarios: from macro stick–slip to continuous sliding. Meccanica **50**, 649–664 (2015). https://doi.org/10.1007/s11012-014-0010-2
49. Khajeh Salehani, M., Irani, N., Nicola, L.: Modeling adhesive contacts under mixed-mode loading. J. Mech. Phys. Solids **130**, 320–329 (2019). https://doi.org/10.1016/j.jmps.2019.06.010
50. Wang, Y., Meng, Z.: Mechanical and viscoelastic properties of wrinkled graphene reinforced polymer nanocomposites–effect of interlayer sliding within graphene sheets. Carbon NY **177**, 128–137 (2021). https://doi.org/10.1016/j.carbon.2021.02.071
51. Xu, R.-G., Zhang, G., Xiang, Y., Garcia, J., Leng, Y.: Will Polycrystalline platinum tip sliding on a gold(111) surface produce regular stick-slip friction? Langmuir **38**, 6808–6816 (2022). https://doi.org/10.1021/acs.langmuir.1c03268
52. Yau, S.Y., Yoo, S.S., Penkov, O.V., Kim, D.E.: Wear reduction of borosilicate glass microballs using vapor-phase lubrication with n-Pentanol. Tribol. Trans. **59**, 507–512 (2016). https://doi.org/10.1080/10402004.2015.1090044
53. Sawyer, W.G., Blanchet, T.A.: Vapor-phase lubrication in combined rolling and sliding contacts: modeling and experimentation. J. Tribol. **123**, 572–581 (2000). https://doi.org/10.1115/1.1308039
54. Müser, M.H., Urbakh, M., Robbins, M.O.: Statistical mechanics of static and low-velocity kinetic friction. Adv. Chem. Phys. **126**, 187–272 (2003)
55. Riedo, E., Gnecco, E., Bennewitz, R., Meyer, E., Brune, H.: Interaction potential and hopping dynamics governing sliding friction. Phys. Rev. Lett. **91**, 84502 (2003). https://doi.org/10.1103/PhysRevLett.91.084502
56. Popov, V.L., Gray, J.A.T.: Prandtl–Tomlinson model: a simple model which made history BT. In: Stein, E. (ed.) The History of Theoretical Material and Computational Mechanics-Mathematics Meets Mechanics and Engineering, pp. 153–168. Springer, Berlin, Heidelberg (2014)
57. Shi, B., Gan, X., Yu, K., Lang, H., Cao, X., Zou, K., Peng, Y.: Electronic friction and tuning on atomically thin MoS2. npj 2D Mater. Appl. **6**, 39 (2022). https://doi.org/10.1038/s41699-022-00316-6
58. Gianetti, M.M., Guerra, R., Vanossi, A., Urbakh, M., Manini, N.: Thermal friction enhancement in Zwitterionic monolayers. J. Phys. Chem. C **126**, 2797–2805 (2022). https://doi.org/10.1021/acs.jpcc.1c09542
59. Li, Q., Dong, Y., Perez, D., Martini, A., Carpick, R.W.: Speed dependence of atomic stick-slip friction in optimally matched experiments and molecular dynamics simulations. Phys. Rev. Lett. **106**, 126101 (2011). https://doi.org/10.1103/PhysRevLett.106.126101
60. Lowrey, D.D., Tasaka, K., Kindt, J.H., Banquy, X., Belman, N., Min, Y., Pesika, N.S., Mordukhovich, G., Israelachvili, J.N.: High-speed friction measurements using a modified surface forces apparatus. Tribol. Lett. **42**, 117–127 (2011). https://doi.org/10.1007/S11249-011-9746-1
61. van der Bondi, A.: Waals volumes and radii. J. Phys. Chem. **68**, 441–451 (1964). https://doi.org/10.1021/j100785a001
62. Ramírez-Zavaleta, F.I., Torres-Dominguez, V.M., Viramontes-Gamboa, G., Rivera, J.L.: Interfacial forces in free-standing layers of melted polyethylene, from critical to nanoscopic thicknesses. Polymers (Basel) **14**, 3865 (2022)
63. Peña-Obeso, P.J., Huirache-Acuña, R., Ramirez-Zavaleta, F.I., Rivera, J.L.: Stability of non-concentric, multilayer, and fully aligned porous MoS2 nanotubes. Membranes (Basel) **12**, 818 (2022)

Authors and Affiliations

Roberto Guerra-Gonzalez[1] · Vidal Moises Bastida-Silva[2] · Jose Luis Rivera[3] · Fernando Iguazu Ramirez-Zavaleta[2] · Enrique Lima[3]

✉ Jose Luis Rivera
jlrivera@umich.mx

[1] Facultad de Ingeniería Química, Universidad Michoacana de San Nicolás de Hidalgo, 58000 Morelia, Michoacán, México

[2] Facultad de Ciencias Físico - Matemáticas, Universidad Michoacana de San Nicolás de Hidalgo, 58000 Morelia, Michoacán, México

[3] Laboratorio de Fisicoquímica Y Reactividad de Superficies (LaFReS), Instituto de Investigaciones en Materiales, Universidad Nacional Autónoma de México, Circuito Exterior S/N, CU, Del. Coyoacán, Ciudad de Mexico, México